POLITECNICO
MILANO 1863

DIPARTIMENTO DI MECCANICA

mecc

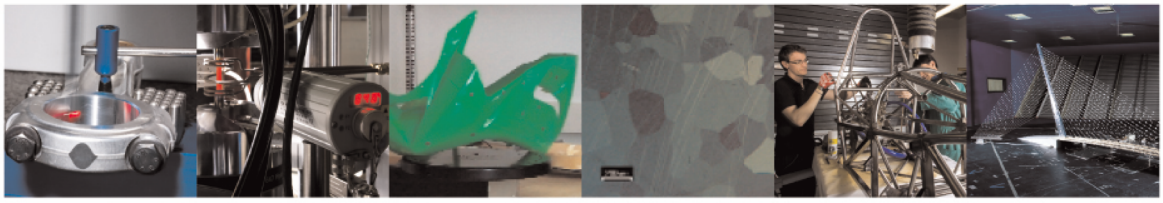

Ad Hoc Heat Treatments for Selective Laser Melted Alsi10mg Alloy Aimed at Stress-Relieving and Enhancing Mechanical Performances

Fiocchi J.;Biffi C. A.;Colombo C.;Vergani L. M.;Tuissi A.

This version of the article has been accepted for publication, after peer review (when applicable) and is subject to Springer Nature's AM terms of use, but is not the Version of Record and does not reflect post-acceptance improvements, or any corrections. The Version of Record is available online at: https://doi.org/10.1007/s11837-019-03973-z

Ad-hoc heat treatments for selective laser melted AlSi10Mg alloy aimed at stress relieving and enhancing mechanical performances

J. Fiocchi[1], C.A. Biffi[1*], C. Colombo[2], L. M. Vergani[2], A. Tuissi[1]

[1] CNR ICMATE; National Research Council, Institute of Condensed Matter Chemistry and Technologies for Energy, Unit of Lecco; Via Previati 1/e, 23900 Lecco, Italy.

[2] Department of Mechanical Engineering, Politecnico di Milano, via La Masa 1, 20156 Milano, Italy.

* corresponding author: carloalberto.biffi@cnr.it

JOM, Vol. 72, No. 3, 2020, SpringerNature

https://doi.org/10.1007/s11837-019-03973-z

Licence: CC BY-NC-ND

Abstract

In the present work the response of an AlSi10Mg alloy produced by selective laser melting (SLM) to specifically designed heat treatments is explored. Thermal phenomena of the rapidly solidified material were studied by differential scanning calorimetry (DSC) and the results were used to define specific post processing thermal treatment temperatures. In details, three heat treatments were studied: two innovative ones, able to selectively trigger i) Mg_2Si precipitation and ii) the rupture and spheroidization of the silicon network, and iii) a T5-like ageing were applied for different times and their effect on mechanical properties was studied. The first and the second heat treatments were selected by combining DSC analysis and aging curves for the optimization of the temperature and duration and these were more deeply investigated in terms of microstructural evolution and of residual stresses. The optimized thermal treatments for SLM built AlSi10Mg are recommended as valid alternative to the usually applied T6 or high-temperature stress release treatments.

Keywords

Selective Laser Melting; aluminum alloy; thermal treatment; mechanical behavior; microstructure; residual stresses; AlSi10Mg.

1. Introduction

Selective laser melting (SLM), belonging to the family of additive manufacturing processes, has gained in the last few years a good degree of industrial maturity and widespread availability thanks to its well-known advantages. Currently, Si-based aluminum alloys, and in particular the age-hardenable AlSi10Mg and AlSi7Mg, have been widely studied thanks to their low shrinkage and melting temperature and acceptable weldability. Their microstructural features, as well as the deriving mechanical properties, radically differ from the ones of conventionally produced materials because of the intrinsic peculiarities of the additive manufacturing process. This is made more complex in the case of using multi lasers incident on the same areas [1]. When two or more laser beams scan the same portion of powder, higher amount of spatter can be generated and this can promote the formation of defects [2]. The printability of the AlSi10Mg alloy was tested using the multi laser approach in few works: it was found that the overlapping of two laser beams can induce lower relative density, due to higher porosity and spatter formation, thus reducing the mechanical properties [3,4].

In SLM-built parts, the high power density incident on the melt pool locally leads to high heating and cooling rates [5], which result in residual stresses, very fine microstructure and solid solubility extension, that strongly affect the material properties. Similar microstructural results were achieved by using other AM processes, like micro laser deposition with a thin wire of AlSi alloy [2].

Hence thermal treatments, which are commonly applied to alloys produced by conventional processes, may not be suitable for the SLMed materials. Cast AlSi10Mg alloy is usually subjected to a thermal treatment based on solution treatment and artificial ageing in order to achieve strengthening through precipitation. However, for SLM-built parts these treatments shall be properly tuned, or even substituted by new ones, in order to obtain a balanced set of mechanical performances. Moreover, thermal annealing should be considered as a standard post-processing operation for SLM products, since it is of paramount importance in removing residual stresses, which may induce distortions and micro cracks [7,8]. Hence, increasing attention has been recently devoted to defining proper thermal treatments for SLM-built AlSi10Mg parts. Two approaches were found to be the most accepted in the literature: in the first case T6 (solution treatment followed by artificial ageing) or T5 (artificial ageing) treatments were adapted, in terms of temperature and

duration, to SLM products in order to strengthen the alloy by precipitation hardening. In the second case annealing at various temperatures, usually lying between ageing and solution treatment ones, were tested in order to obtain stress relieving and an improvement of the material ductility.

Numerous works reported that traditional T6 treatment leads to a sharp decrease in strength of the material, but on the other side allows obtaining a good ductility [9–11]. An improvement of tensile strength with respect to the base material was obtained by T5 treatment at various temperatures [12]. Some authors [13–16] performed a deep microstructural characterization of treated AlSi10Mg alloy and found out that heat treatment only marginally affected grain size, but could induce the nucleation of some smaller equiaxed grains at melt pool boundaries. Moreover, solution treatment at temperatures above 500°C was found to cause the formation of needle-like Al_5FeSi precipitates, which are known to be detrimental for the mechanical behavior of the alloy. Several authors reported that T6-like treatments were able to homogenize the microstructure of SLM–built samples, thus also reducing the anisotropy, which arises from the layer by layer building strategy [17–19].

The effect of the second group of thermal treatments, i.e. the ones aimed at obtaining an improvement of the material ductility, was also widely studied. Annealing at temperatures higher than 200 °C allowed to break the Si network and increase ductility [20-22]. Toughness and fatigue resistance of SLM–built parts were also found to be tunable thanks to heat treatments at various temperatures [23-27].

Finally, thermal treatments based on results from calorimetric analyses of the as-built samples were proposed by the authors of the present paper [28] and by Yang et al. [29].

The present work proposes to correlate the effect of temperature and time of thermal treatments dedicated to SLMed AlSi10Mg alloy on the mechanical and microstructural features. These treatments are formulated on the basis of DSC analysis and aging curves for the optimization of the temperature and duration: their aim is to offer a valid alternative to the traditional T6 treatment or to high-temperature stress release treatments. Moreover, T5 treatment aimed at obtaining precipitation hardening is implemented. The evolution of mechanical properties is correlated to microstructural changes and stress relieving phenomena occuring upon annealing.

2. Materials and experimental procedure

Gas atomized AlSi10Mg powders, whose chemical composition is reported in [28], were used. The powder featured a particles size between 20 µm and 63 µm with average size of approximately 45 µm.

Samples were produced by means of an SLM Solutions (model 500 HL quad 4 × 400 W) system. Standard process parameters were used: laser power 350 W, scanning speed 1.15 m/s, spot size 80 µm, building plate temperature 150 °C, layer thickness 50 µm, hatch distance 170 µm. Specimens were built, using the stripes scanning strategy, with their main axes lying both on the horizontal (xy) and vertical (xz) planes, as shown in the insert in Figure 1 b.

Density of the samples was checked by Archimedes' principle and was found to be fully satisfactory (> 99 %). Thermal analyses were carried out by differential scanning calorimetry (DSC, mod. Seiko DSC220C) to detect the thermal signals related to phase transformations and precipitation phenomena in the SLM-built alloy. The tests were performed in the temperature range 0-500 °C, with heating rates of 5, 10, 20 and 30 °C/min. The data collected at different heating rates were used to calculate the temperatures, below and above the peaks of the phase transformations, for implementing isothermal heat treatments, specifically designed on the SLM built AlSi10Mg alloy.

As a result of the previous DSC analysis, thermal treatments were carried out at the calculated temperatures for times ranging from 10 min to 7 hrs. Moreover, a T5-like heat treatment at 170 °C was explored in the same time interval for comparison. After annealing samples were naturally cooled in air.

The evolution of mechanical properties on all the samples was evaluated by Vickers microhardness and tensile testing on standard dog-bone specimens (ASTM E8M). A Future Tech Corporation FM-700 hardness tester (300 g load, for 15 s, on xy sections) and a MTS 2/M machine equipped with extensometer (strain rate of 0.015 min^{-1}) were used for hardness and tensile tests, respectively. Morphological analysis of the microstructure, before and after heat treatment, was carried out by means of a scanning electron microscope (SEM, mod. Leo 1413) operating at 20 KV on polished sections with XY orientation. DSC tests were performed at 10 °C/min on heat treated samples in order to follow the evolution of the on-going transformations. Residual stresses were measured with an XRD diffractometer (AST X-Stress 3000) on thin plates (100 x 40 x 1

mm^3). The measurement parameters, determined by the sin2ψ method, were: collimator with 3 mm diameter, Cr Kα X-ray tube with voltage 30kV and current 6.7 mA, 9 points for the diffraction angles, exposure time 25 s. All the measurements were performed at the specimen surface, given the reduced thickness of these plates.

3. Results and discussion

3.1 Microstructure and mechanical behavior of the as built samples

The microstructure of as-built samples (Figure 1a) was characterized by the typical fine structure induced by rapid cooling. Silicon formed an interconnected fine network surrounding the Si rich aluminum matrix and no trace of the harmful needle-like Al_5FeSi was found. The resulting mechanical properties are shown in Figure 1b for samples built on both xy and xz planes. Measured yield stress was 288 MPa and 271 MPa (± 5 MPa) for xy and xz samples, whereas ultimate tensile strength was 414 MPa and 419 (± 7 MPa), respectively. Elongation to failure was 5.6 % and 4.1 % (±0.2 %) for the two batches of samples. The earlier failure of xz samples has been ascribed to different causes, including the building layers being perpendicular to the pulling direction, pores being more numerous due to the higher number of layers, residual stresses building up along z direction [30]. A comparison of the mechanical properties of SLMed samples, industrial reference values, and the cast alloy is shown in Figure 1c.

3.2 Calorimetric analysis for the definition of heat treatment temperatures

A DSC scan of the as built material is shown in Figure 2a. Two characteristic exothermic signals, lying at 259 °C and 321 °C, were visible. The first one, which is characterized by higher intensity, was related to the precipitation of the reinforcing Mg_2Si precipitate in its coherent β'' form. The second peak was initially described by the authors of the present work as connected to the rupture and spheroidization of Si network [30]. This explanation was partially modified in [31] (1^{st} peak was attributed to Si precipitation) but confirmed in [32] and [33]. However, due to the asymmetric shape of the signal and to findings which will be presented in the following sections, it is now proposed that peak 2 results from the overlapping of two signals, which

are related to two distinct phenomena: the transformation of β'' precipitates into the β' form and the rupture and spheroidization of Si network. As graphically shown in Figure 2b, and in accordance with Daoudi et al. [34], β' formation contributes to the first part of the peak (peak temperature at about 320 °C), whereas Si spheroidization takes place in its last part (peak temperature at about 340 °C).

The endpoint temperatures of each peak were used in order to define heat treatments, which could selectively induce either β'' precipitation or Si spheroidization. By applying the same procedure described in [28], the endpoint temperature of the transformations during isothermal treatments were computed to be 244 °C and 289 °C for peak 1 and 2, respectively. It should be noted that these temperatures differ from the ones, that were obtained in [28]. This shift shall be ascribed to the different processing conditions of the samples used in the present paper: as already demonstrated and reported elsewhere [35,36], the processing parameters) and the laser emission strategy can heavily affect the microstructure and the thermal properties of SLM–built AlSi10Mg parts.

3.3 Mechanical properties evolution for the definition of heat treatment durations

The endpoint temperatures computed in section 3.1 were used in order to assess the answer of the SLM-built aluminum samples to heat treatments at different temperatures. Moreover, a more traditional T5-like ageing treatment was applied. In summary, the following experiments were carried out, for times ranging from 10 min to 7 hrs:

- T = 170 °C (T5-like), aimed at inducing precipitation hardening
- T = 244 °C (above peak 1), aimed at stress relieving the material while retaining acceptable hardness thanks to precipitation of β''
- T = 290 °C (above peak 2), aimed at increasing the material's ductility thanks to the rupture of Si network

The hardness trends of SLM-built samples as function of ageing time during holding at the three considered temperatures are reported in Figure 3. Ageing at 170 °C showed a quite typical behavior of age-hardenable aluminum alloys: after an initial small decrease in hardness from 138 HV to 135 HV, caused by a partial

relaxation of residual stresses, a slight increase up to 145 HV was induced by the precipitation of β'' phase. After peak hardness at 90 min, the evolution of coherent precipitates into semi-coherent β' and finally fully incoherent β caused overageing and consequently a hardness decrease. Nevertheless, hardness values for long time ageing were still comparable to the ones typical of material in as-built condition. If compared to the behavior of an AlSi10Mg alloy produced by conventional casting [37], it may be noted that a smaller initial increase is induced in the SLM-built alloy and that peak hardness is reached for much shorter times. This acceleration of ageing process was presumably caused by the fine microstructure and high amount of defects induced by rapid solidification, which may assist Mg and Si atoms in diffusing across aluminum matrix.

During annealing a 244 °C hardness was first slightly increased due to β'' precipitation (10 min), then it smoothly decreased down to 105 HV at 180 min and remained constant for longer ageing times. Finally, heat treatment at 290 °C caused an immediate sharp drop of hardness during the first hour (80 HV). For longer times hardness remained substantially stable at about 74 HV.

A deeper characterization of the evolution of mechanical properties was obtained by performing tensile tests on samples built both in the xy and xz planes. In the present section, the attention is focused on the selection of the optimal heat treatment time. Specimens for the tensile tests underwent thermal treatments with: 1) a short time (10 min); 2) the peak/stabilization point in hardness curves (i.e. 90 min for T=170 °C, 180 min for T=244 °C and 45 min for T=290 °C); and 3) a long time (300 min). Figure 4 reports the results of the tests, in terms of Yield Stress (YS), Ultimate Tensile Strength (UTS) and Elongation to failure (Ef). Moreover, Figure 5 reports complete stress-strain curves of both xy and xz samples in the peak/stabilization conditions. As expected, yielding stress and ultimate tensile strength values followed tightly the trends of hardness in Figure 3. Moreover, the influence of heat treatment times and temperatures on the tensile behavior was quite constant, regardless the orientation along which the samples had been built. As far as elongation to failure is concerned, ageing at 170 °C caused a deterioration of performance since very short times. The same decrease was induced for short times by treatment at 244 °C. However, for longer durations ductility rose again, finally restoring as-built performances or even improving them. Holding at 290 °C induced the largest improvement in elongation to failure, allowing to reach almost 10 % elongation after a 5 hrs treatment. It should be noted that only holding at 290 °C induced a continuous increase in elongation to failure, even for

longer times, likely because of the progressive coarsening of Si particles, which went on after the rupture of the original network. Samples built on xz plane were characterized by a slightly lower ductility in as-built conditions and in the first stages of heat treatment, but the difference became smaller for long annealing times. This is believed to be caused by the fact that in xz samples the load is applied perpendicularly to the layers composing the specimen, thus detaching them. After heat treatment, especially at high temperature, the microstructure of the sample was homogenized, thus reducing the problems connected to adhesion between different layers and leading to a more uniform behavior.

3.4 Performances of the optimized heat treatments

According to the results reported in paragraphs 3.2 and 3.3, the following temperature/time combinations were selected as the optimal ones and were subjected to deeper characterization: 1) 170 °C for 90 min (T5-like), 2) 244 °C for 180 min (stress relieve) and 3) 290 °C for 45 min (ductility increase).

Figure 5 shows the stress-strain curves of the heat treated samples. The two annealing treatments at 244°C and 290°C have a similar effect, as the curves are very near, while the T5-like treatment at 170°C results in higher yield stress and ultimate tensile strength, but also in lower elongation to failure, especially considering xz specimens.

It is important to get information regarding the evolution of the residual stresses as function of the identified heat treatments. For the sake of completeness, residual stresses were measured in as built and heat treated conditions. Stresses were measured along the in-plane directions in the center of each specimen, then principal stresses were calculated and reported in Figure 6.

For the as-built configuration only, X-ray measurements collected along samples' height (i.e. along x for xy samples and along z for xz samples) revealed that residual stresses are dependent on the position. Focusing on the single stress components, the highest values are along z direction, normal to the building plate, while in the other in-plane directions stresses are less than a half. This means that z axis is approximately also the direction of the maximum principal stress. Further details on these measurements are reported in [38].

The maximum principal residual stresses $\sigma_{p,max}$ in as-built configuration are the highest, with values of 97 and 85 MPa respectively in xy and xz samples (see Figure 6). These are not negligible, as they are respectively

23% and 20% of their UTS (see Section 3.1). The minimum principal stresses, which are near to zero or slightly in compression, are less meaningful. These values are in accordance with literature ones [39,40] .

It may be appreciated that the trend of $\sigma_{p,max}$ is deeply affected by the treatment temperature . In particular, the 170°C treatment decreases $\sigma_{p,max}$ of -48% for xy samples and -24% for xz samples, when compared to the as-built condition.

On the other hand, the thermal treatments at 244°C and 290°C seem very effective, because $\sigma_{p,max}$ is decreased to about -80%. The residual stresses $\sigma_{p,max}$ after the three thermal treatments are low and quite similar, having intersecting confidence bands. In particular, xy samples have confidence bands intersecting the zero stress value, while xz sample still have very little residual stress values (around 30MPa for the 244°C and 290°C treatments), near to the accuracy of the X-Ray diffractometer, which is approximately 10 MPa. Therefore, it can be stated that the thermal treatments at 244°C for 180min and at 290°C for 45min, that were selected based on the calorimetric analysis of Section 3.1, result in similar residual stresses. In other words, it seems that an effective stress relieve happens at temperatures similar to the ones which were meant to induce Mg_2Si precipitation. Nevertheless, these two processes shall be considered as unrelated, since it is well known that the formation of coherent precipitates, such as β'', usually induce the buildup of local stress in the aluminum matrix [41]. On the other hand, Si network breaking and spheroidization induced at 290°C (above peak 2 in Figure 2) is almost not further affecting residual stresses. Hence, we can underline that the proposed thermal treatment at 244 °C has the same effect, but at lower temperature than the thermal treatment at 290 °C. Moreover, it shall be noticed that an even greater advantage is obtained over standard treatments of SLM-built AlSi10Mg parts, which are usually carried out in the 300 °C - 320°C range [28,38]. This is an important observation for the optimization of the thermal post-processing of these AlSi10Mg samples, and, in particular, for time and energy savings.

In order to better understand the evolution of mechanical properties the concurrent microstructural evolution was characterized by SEM and DSC. Figure 7 reports the micrographs of samples subjected to the previously selected temperature/time combinations. Micrographs of samples treated for different times are reported in the supporting materials (Figure S1). It is evident that treatments performed at 170 °C and 244 °C induced only a limited evolution of microstructure: no β'' and β' precipitates were visible, since they are

too fine to be detected by SEM at the considered magnifications and no rupture of the Si network was induced. The integrity of the Si structure and the size of the Si cells are maintained even for long durations, thus allowing the retaining of relatively high mechanical strength. On the contrary, annealing at 290 °C induced an evident Si network breaking and Si spheroidization since the very first stages. For low treatment times, evident traces of the preexisting cellular structure are still visible in the distribution of the Si particles: upon heat treatment, Si is likely rejected from the supersaturated matrix and particles precipitate along the Al-Si cellular interfaces, thus keeping memory of the disappearing structure [21]. With prolonged holding at high temperature, the particles grow by Ostwald ripening, giving rise to coarser and more distanced Si particles, which are less efficient in impeding dislocations motion [10,12,42].

Calorimetric analyses, whose results are reported in Figure 8, allowed a deeper understanding of the microstructural evolution upon annealing. For the sake of simplicity, peak 2 was not deconvoluted in order to distinguish the contributions arising from β' and Si transformations. However, the trends emerging from the experiments allowed to understand how each phenomenon participated in the exothermic peak. Ageing at 170 °C induced a rapid decrease of enthalpy of peak 1 in the first 45 min; thereafter a much smoother decrease took place until a final value of 3.2 mJ/mg was reached after 300 min. Peak 2 was characterized by an initial shallow reduction of enthalpy which, after 45 min, started slowly increasing again. These results, accordingly with hardness results, confirm that the majority of β'' precipitation took place for short times. The stability of peak 2 suggests that Si was not affected by the treatment, whereas the slight enthalpy increase may indicate that the progressive formation of β'' precipitates supports their successive transformation into the following β' phase [43].

As far as annealing at 244 °C is concerned, it may be immediately appreciated that peak 1 almost disappeared after a 30 min treatment, whereas peak 2 showed a more complex behavior: after an initial decrease, enthalpy grew up to a maximum (8.1 mJ/mg at 120 min) and then went back to values, which were comparable to the original ones. It is likely that during the first two hours β' formation becomes progressively easier thanks to the rapid precipitation of β'', which is taking place. For longer annealing times the transformation from β'' to β' takes place, thus progressively reducing the dimensions of the peak. The contribution to the peak, which remains substantially constant all along the thermal treatment may be

ascribed to the rupture of Si network, which, as clearly shown in Figure 7, never takes place at 244 °C. It may be inferred that the initial very short hardness increase was caused by precipitation of β', then concurrent stress relief and β'' formation induced a progressive weakening. The deterioration of mechanical properties did not proceed further thanks to the presence of the Si network, which was left unchanged.

Annealing at 290 °C caused an even faster disappearance of peak 1 (0 mJ/mg at 45 min). A similar trend, only slightly retarded, was shown by peak 2. This behavior perfectly fits the one of microhardness, which reached almost complete stability after 45 min. The same can be said about SEM micrographs, which show that most of the Si network had already disappeared after 45 min.

4 Conclusions

The present work explored the response of AlSi10Mg parts produced by Selective Laser Melting to thermal treatments, which were specifically designed starting from the inherent thermal properties of the alloy. Treatment temperatures and durations were successfully computed by coupling calorimetric results and aging curves. These were found able to selectively trigger the desired transformations in the material. Calorimetric analysis also proved to be a powerful method in following the trend of the alloy microstructure and supporting the understanding of the evolution of mechanical properties.

Annealing the alloy at 244 °C (above β'' precipitation peak) allowed to effectively stress relieve the material without losing excessive strength with respect to the as-built condition. This was made possible by retaining the presence of the continuous Si network, which was not broken. On the contrary, the 290 °C treatment was able to break the network and spheroidize the resulting Si particles, thus giving rise to improved ductility. As a drawback also β' formation was triggered causing over-ageing.

Finally the T5-like ageing at 170 °C was able to slightly improve the mechanical resistance of the AlSi10Mg samples for short treatment durations thanks to precipitation of β'' from the supersaturated solid solution. Hence these treatments appear as a valid alternative to the traditional T6 treatment, as far as they can offer improved mechanical performances while requiring lower treatment temperatures and times.

The 244 °C heat treatment appears as a large improvement over the 300°C – 320°C treatments usually applied to SLM built aluminum parts, since it is able to obtain the same stress relieving at much lower temperatures.

Acknowledgments

The authors would like to thank Giordano Carcano from CNR ICMATE and Simone Galli from Politecnico di Milano for their assistance and support in the experiments. The authors would like to acknowledge Accordo Quadro CNR/Regione Lombardia n. 3866 at 17/07/2015 FHfFC for financial support.

References

[1] Andreas Wiesnera, Dieter Schwarzea, Multi-Laser Selective Laser Melting, 8th International Conference on Photonic Technologies LANE 2014.

[2] Mohammad Masoomi, Scott M. Thompson, Nima Shamsaei, Quality part production via multi-laser additive manufacturing, Manufacturing Letters 13 (2017) 15-20.

[3] Changchun Zhang, Haihong Zhu, Zhiheng Hu, Luo Zhang, Xiaoyan Zeng, A comparative study on single-laser and multi-laser selective laser melting AlSi10Mg: defects, microstructure and mechanical properties, Materials Science and Engineering: A 746 (2019) 416-423.

[4] Mohsen Taheri Andani, Reza Dehghani, Mohammad Reza Karamooz-Ravari, Reza Mirzaeifar, Jun Ni, Spatter formation in selective laser melting process using multi-laser technology, Materials & Design 131 (2017) 460-469.

[5] H. Zhang, H. Zhu, T. Qi, Z. Hu, X. Zeng, Selective laser melting of high strength Al – Cu – Mg alloys : Processing , microstructure and mechanical properties, Mater. Sci. Eng. A. 656 (2016) 47–54.

[6] A.G. Demir, C.A. Biffi, Micro laser metal wire deposition of thin-walled Al alloy components: Process and material characterization, J. Manuf. Process. 37 (2019) 362–369.

[7] M.L. Montero, R. Mertens, B. Vrancken, X. Wang, B. Van Hooreweder, J. Kruth, J. Van Humbeeck, Changing the alloy composition of Al7075 for better processability by selective laser melting, J. Mater. Process. Tech. 238 (2016) 437–445.

[8] P. Mercelis, J. Kruth, Residual stresses in selective laser sintering and selective laser melting, Rapid Prototyp. J. 5 (2006) 254–265.

[9] B. Vrancken, K. Kempen, L. Thijs, J.-P. Kruth, J. Van Humbeeck, Adapted heat treatment of selective laser melted materials, Euro PM 2014 Congr. Exhib. Proc. (2014).

[10] N.T. Aboulkhair, I. Maskery, C. Tuck, I. Ashcroft, N.M. Everitt, The microstructure and mechanical properties of selectively laser melted AlSi10Mg: The effect of a conventional T6-like heat treatment, Mater. Sci. Eng. A. 667 (2016) 139–146.

[11] L. Girelli, M. Tocci, L. Montesano, M. Gelfi, A. Pola, Optimization of heat treatment parameters for additive manufacturing and gravity casting AlSi10Mg alloy, IOP Conf. Ser. Mater. Sci. Eng. 264 (2017).

[12] M. Fousová, D. Dvorský, A. Michalcová, D. Vojtěch, Changes in the microstructure and mechanical properties of additively manufactured AlSi10Mg alloy after exposure to elevated temperatures, Mater. Charact. 137 (2018) 119–126.

[13] L. Zhou, A. Mehta, E. Schulz, B. McWilliams, K. Cho, Y. Sohn, Microstructure, precipitates and hardness of selectively laser melted AlSi10Mg alloy before and after heat treatment, Mater. Charact. 143 (2018) 5-17.

[14] K. V. Yang, P. Rometsch, C.H.J. Davies, A. Huang, X. Wu, Effect of heat treatment on the microstructure and anisotropy in mechanical properties of A357 alloy produced by selective laser melting, Mater. Des. 154 (2018) 275–290.

[15] U. Tradowsky, J. White, R.M. Ward, N. Read, W. Reimers, M.M. Attallah, Selective laser melting of AlSi10Mg: Influence of post-processing on the microstructural and tensile properties development, Mater. Des. 105 (2016) 212–222.

[16] N. Takata, H. Kodaira, K. Sekizawa, A. Suzuki, M. Kobashi, Change in microstructure of selectively laser melted AlSi10Mg alloy with heat treatments, Mater. Sci. Eng. A. 704 (2017) 218–228.

[17] L. Hitzler, A. Charles, A. Öchsner, The influence of post-heat-treatments on the tensile strength and surface hardness of selective laser melted AlSi10Mg, Defect Diffus. Forum. 370 (2017) 171–176.

[18] P. Delroisse, P.J. Jacques, E. Maire, O. Rigo, A. Simar, Effect of strut orientation on the microstructure heterogeneities in AlSi10Mg lattices processed by selective laser melting, Scr. Mater. 141 (2017) 32–35.

[19] T. Kimura, T. Nakamoto, Microstructures and mechanical properties of A356 (AlSi7Mg0 . 3) aluminum alloy fabricated by selective laser melting, JMADE. 89 (2016) 1294–1301.

[20] P. Ma, K.G. Prashanth, S. Scudino, Y. Jia, H. Wang, C. Zou, Z. Wei, Influence of Annealing on Mechanical Properties of Al-20Si Processed by Selective Laser Melting, Metals (Basel). 4 (2014) 28–36.

[21] K.G. Prashanth, S. Scudino, H.J. Klauss, K.B. Surreddi, L. Löber, Z. Wang, A.K. Chaubey, U. Kühn, J. Eckert, L. L??ber, Z. Wang, A.K. Chaubey, U. K??hn, J. Eckert, Microstructure and mechanical properties of Al-12Si produced by selective laser melting: Effect of heat treatment, Mater. Sci. Eng. A. 590 (2014) 153–160.

[22] A. Iturrioz, E. Gil, M.M. Petite, F. Garciandia, A.M. Mancisidor, M. San Sebastian, Selective laser melting of AlSi10Mg alloy: influence of heat treatment condition on mechanical properties and microstructure, Weld. World. 65 (2018) 417–424.

[23] J. Suryawanshi, K.G. Prashanth, S. Scudino, J. Eckert, O. Prakash, U. Ramamurty, Simultaneous enhancements of strength and toughness in an Al-12Si alloy synthesized using selective laser melting, Acta Mater. 115 (2016) 285–294.

[24] I. Rosenthal, R. Shneck, A. Stern, Heat treatment effect on the mechanical properties and fracture mechanism in AlSi10Mg fabricated by additive manufacturing selective laser melting process, Mater. Sci. Eng. A. 729 (2018) 310–322.

[25] N.T. Aboulkhair, I. Maskery, C. Tuck, I. Ashcroft, N.M. Everitt, Improving the fatigue behaviour of a selectively laser melted aluminium alloy: Influence of heat treatment and surface quality, Mater. Des. 104 (2016) 174–182.

[26] A. Tridello, C.A. Biffi, J. Fiocchi, P. Bassani, G. Chiandussi, M. Rossetto, A. Tuissi, D.S. Paolino, VHCF response of as-built SLM AlSi10Mg specimens with large loaded volume, Fatigue Fract. Eng. Mater. Struct. (2018).

[27] A. Tridello, J. Fiocchi, C.A. Biffi, G. Chiandussi, M. Rossetto, A. Tuissi, D.S. Paolino, VHCF response of Gaussian SLM AlSi10Mg specimens: Effect of a stress relief heat treatment, Int. J. Fatigue. 124 (2019) 435–443.

[28] J. Fiocchi, A. Tuissi, P. Bassani, C.A. Biffi, Low temperature annealing dedicated to AlSi10Mg selective laser melting products, J. Alloys Compd. 695 (2017) 3402–3409.

[29] P. Yang, M.A. Rodriguez, L.A. Deibler, B.H. Jared, J. Griego, A. Kilgo, A. Allen, D.K. Stefan, Effect of thermal annealing on microstructure evolution and mechanical behavior of an additive manufactured AlSi10Mg part, Journal of Materials Research 33-12 (2018) 1701-1712.

[30] E.O. Olakanmi, R.F. Cochrane, K.W. Dalgarno, A review on selective laser sintering / melting (SLS / SLM) of aluminium alloy powders : Processing , microstructure , and properties, J. Prog. Mater. Sci. 74 (2015) 401–477.

[31] S. Marola, D. Manfredi, G. Fiore, M.G. Poletti, M. Lombardi, P. Fino, L. Battezzati, A comparison of Selective Laser Melting with bulk rapid solidification of AlSi10Mg alloy, J. Alloys Compd. 742 (2018) 271–279.

[32] A. Aversa, M. Lorusso, F. Trevisan, E. Ambrosio, F. Calignano, D. Manfredi, S. Biamino, P. Fino, M. Lombardi, M. Pavese, Effect of Process and Post-Process Conditions on the Mechanical Properties of an A357 Alloy Produced via Laser Powder Bed Fusion, Metals 7 (2017) 68.

[33] R. Casati, M. Vedani, Aging Response of an A357 Al Alloy Processed by Selective Laser Melting, Adv. Eng. Mater. (2018) 1800406.

[34] M.I. Daoudi, A. Triki, A. Redjaimia, DSC study of the kinetic parameters of the metastable phases formation during non-isothermal annealing of an Al-Si-Mg alloy, J. Therm. Anal. Calorim. 104 (2011) 627–633.

[35] C.A. Biffi, J. Fiocchi, A. Tuissi, Selective laser melting of AlSi10 Mg: Influence of process parameters on Mg2Si precipitation and Si spheroidization, J. Alloys Compd. 755 (2018) 100–107.

[36] C.A. Biffi, J. Fiocchi, P. Bassani, A. Tuissi, Continuous wave vs pulsed wave laser emission in selective laser melting of AlSi10Mg parts with industrial optimized process parameters : Microstructure and mechanical behaviour, Addit. Manuf. 24 (2018) 639–646.

[37] R.X. Li, R.D. Li, Y.H. Zhao, L.Z. He, C.X. Li, H.R. Guan, Z.Q. Hu, Age-hardening behavior of cast Al – Si base alloy, Mater. Lett. 58 (2004) 2096–2101.

[38] C. Colombo, C.A. Biffi, J. Fiocchi, A. Tuissi, L.M. Vergani, Effect of optimized heat treatments on the tensile behavior and residual stresses of selective laser melted AlSi10Mg samples, Key Eng. Mater., 813 (2019) 364-369.

[39] S. Bagherifard, N. Beretta, S. Monti, M. Riccio, M. Bandini, M. Guagliano, On the fatigue strength enhancement of additive manufactured AlSi10Mg parts by mechanical and thermal post-processing, Mater. Des. 145 (2018) 28–41.

[40] A. Salmi, E. Atzeni, L. Iuliano, M. Galati, Experimental analysis of residual stresses on AlSi10Mg parts produced by means of Selective Laser Melting (SLM), Procedia CIRP. 62 (2017) 458–463.

[41] I.J. Polmear, Light alloys: metallurgy of the light metals, John Wiley & Sons Australia, 1995.

[42] W. Li, S. Li, J. Liu, A. Zhang, Y. Zhou, Q. Wei, C. Yan, Y. Shi, Effect of heat treatment on AlSi10Mg alloy fabricated by selective laser melting: Microstructure evolution, mechanical properties and fracture mechanism, Mater. Sci. Eng. A. 663 (2016) 116–125.

[43] I. Dutta, S.M. Allen, A calorimetric study of precipitation in aluminum alloy 6061, J. Mater. Sci. Lett. 10 (1991) 323–326.

List of captions:

Figure 1: a) SEM micrograph of an AlSi10Mg sample in as-built conditions; b) Tensile curves of AlSi10Mg samples built on xy (horizontal) and xz (vertical) planes, in as-built conditions; c) Yield Stress (YS), Ultimate Tensile Strength (UTS) and Elongation to Failure (Ef) of SLMed and cast AlSi10Mg alloy.

Figure 2: a) Representative DSC curve recorded at 10 °C/min of as-built sample; b) deconvolution of the three peaks.

Figure 3: Ageing curves of SLM-built samples collected on isothermal holding at 170 °C, 244 °C and 290 °C.

Figure 4: Yield Stress (YS), Ultimate Tensile Strength (UTS) and Elongation to Failure (Ef) of SLM-built samples subjected to isothermal holding at 170 °C, 244 °C and 290 °C, built on xy (a, b, c) and xz (d, e, f) planes.

Figure 5: Tensile curves of AlSi10Mg samples built on a) xy (horizontal) and b) xz (vertical) planes, in the main heat treated conditions.

Figure 6: Maximum and minimum principal stresses in as-built and heat treated conditions, for xy and xz samples: mean and standard deviation.

Figure 7: SEM micrographs of SLM built samples after heat treatment at 170 °C for 90 min, 244 °C for 180 min and 290 °C for 45 min. All images were taken on the xy plane in the fine fusion zone.

Figure 8: DSC curves recorded at 10 °C/min of samples heat treated for various times at a) 170 °C, b) 244 °C and c) 290 °C. Transformation enthalpies related to peak 1 and peak 2 in samples heat treated for various times at d) 170 °C, e) 244 °C and f) 290 °C.

Figures:

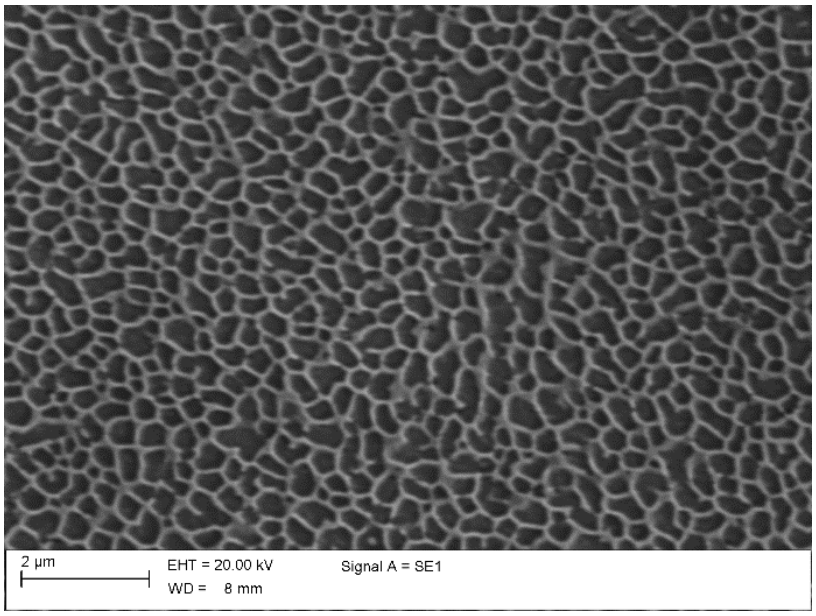
2 µm
EHT = 20.00 kV
WD = 8 mm
Signal A = SE1

(a)

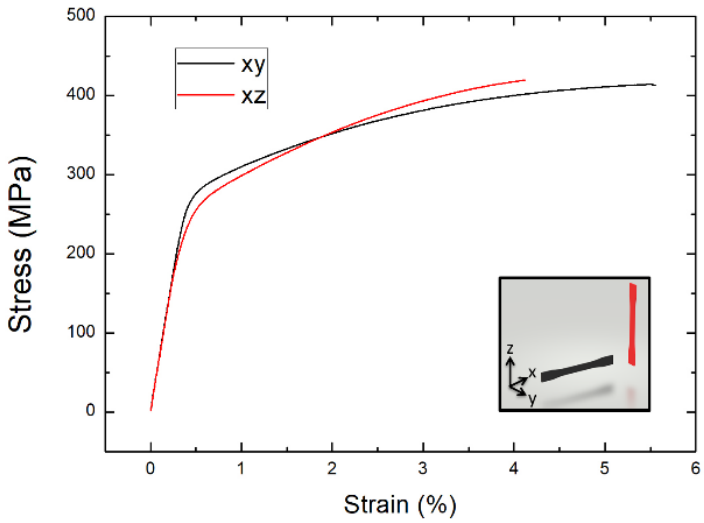
xy
xz
Stress (MPa)
Strain (%)
0
100
200
300
400
500
0
1
2
3
4
5
6
z
x
y

(b)

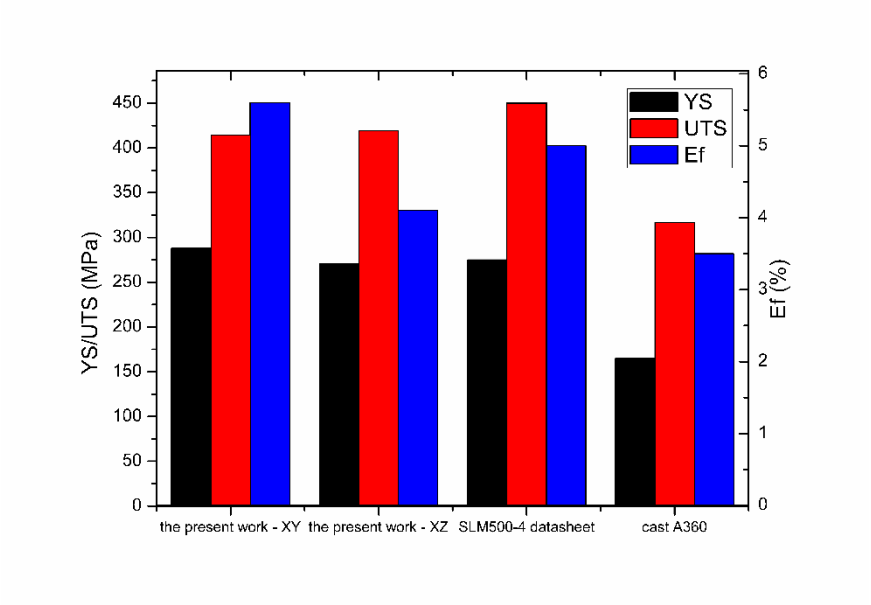

(c)

Figure 1: a) SEM micrograph of an AlSi10Mg sample in as-built conditions; b) Tensile curves of AlSi10Mg samples built on xy (horizontal) and xz (vertical) planes, in as-built conditions; c) Values of the mechanical properties of SLMed and cast AlSi10Mg alloy.

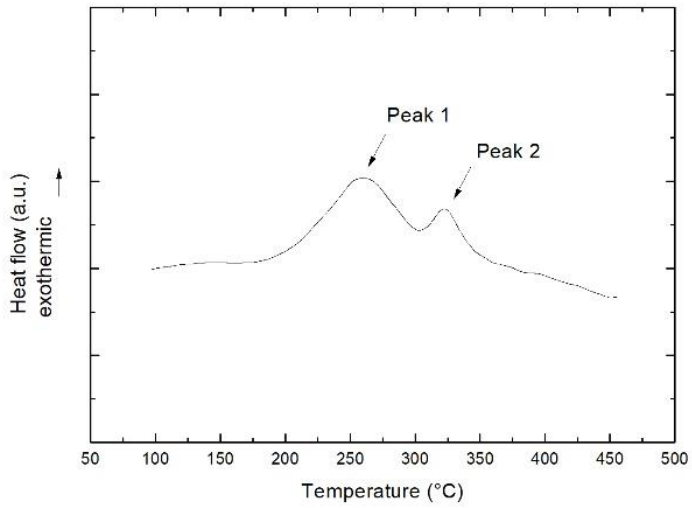

(a)

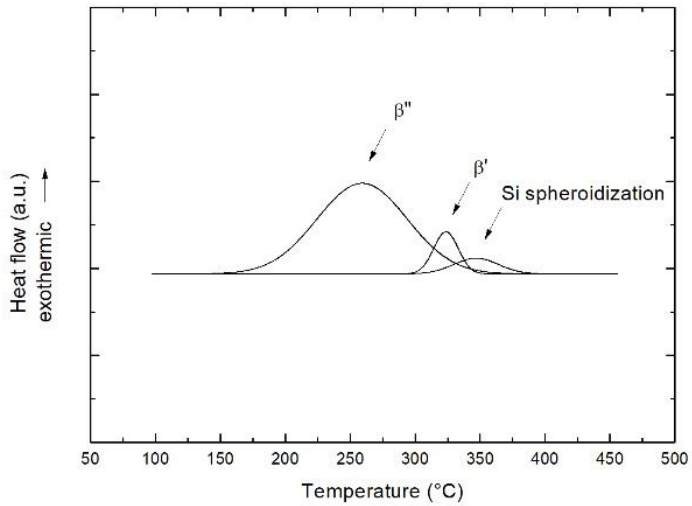

(b)

Figure 2: a) Representative DSC curve recorded at 10 °C/min of as-built sample; b) deconvolution of the three peaks.

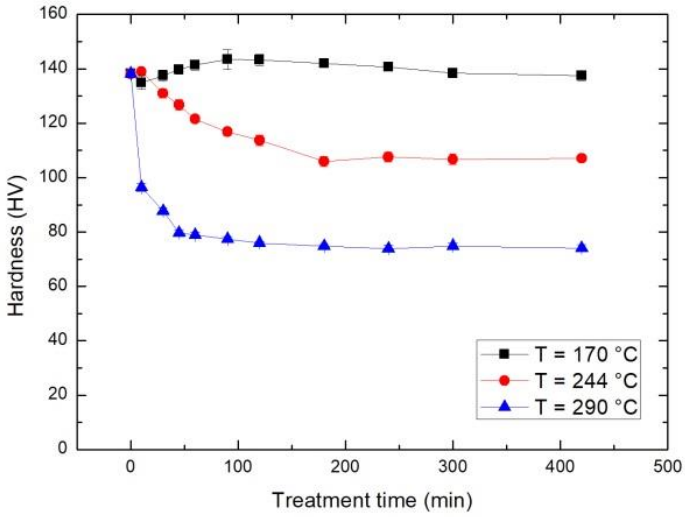

Figure 3: Ageing curves of SLM-built samples collected on isothermal holding at 170 °C, 244 °C and 290 °C.

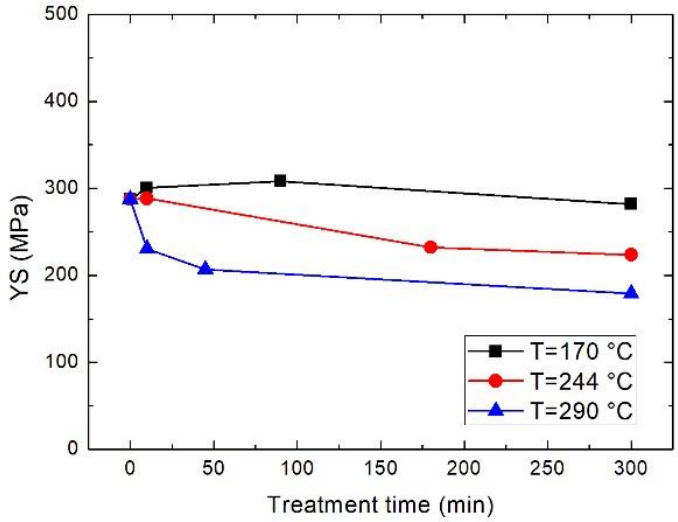
YS (MPa)
Treatment time (min)
T=170 °C
T=244 °C
T=290 °C

(a)

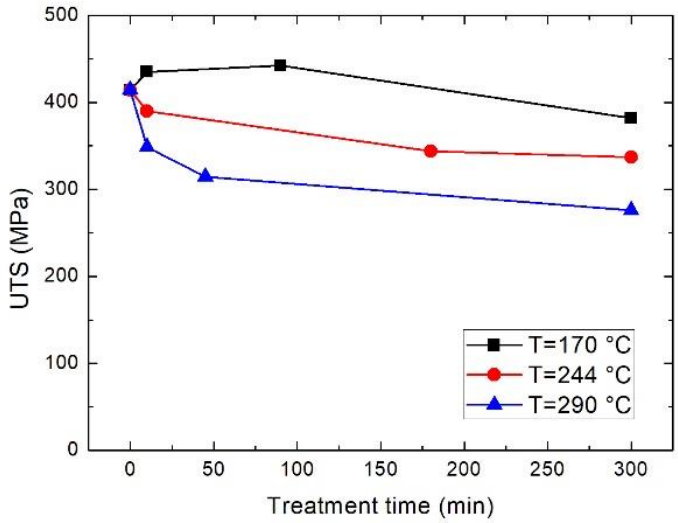
UTS (MPa)
Treatment time (min)
T=170 °C
T=244 °C
T=290 °C

(b)

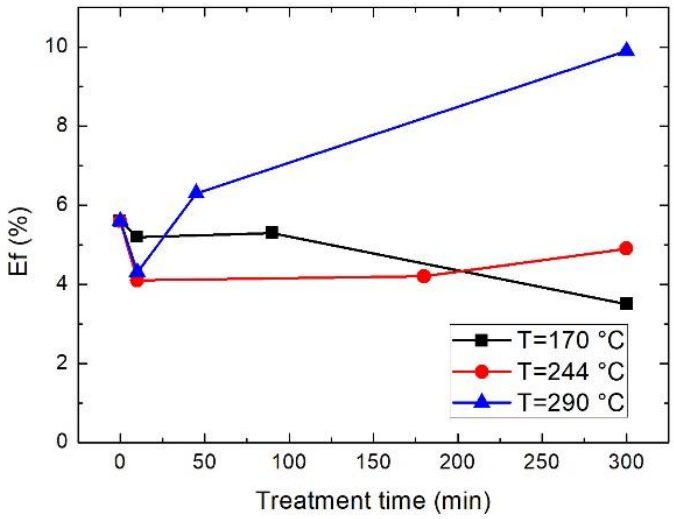
Ef (%)
Treatment time (min)
T=170 °C
T=244 °C
T=290 °C

(c)

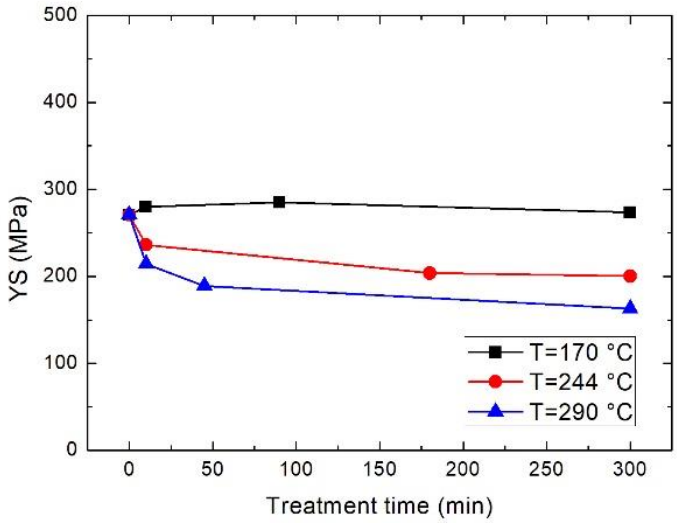
YS (MPa)
Treatment time (min)
T=170 °C
T=244 °C
T=290 °C

(d)

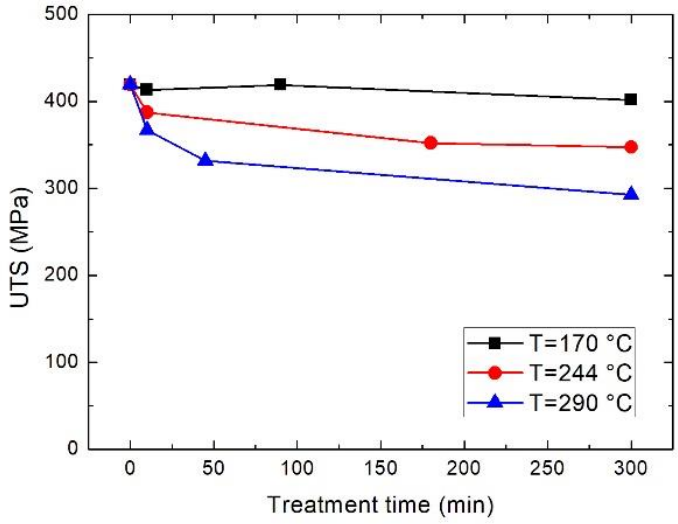

(e)

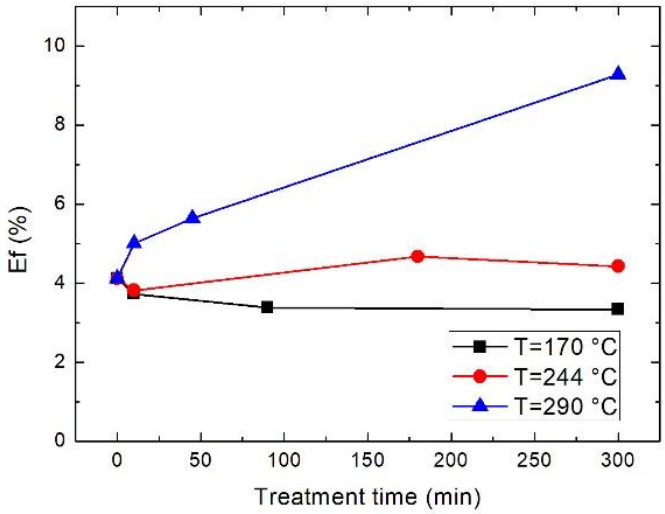

(f)

Figure 4: Yield Stress (YS), Ultimate Tensile Strength (UTS) and Elongation to Failure (Ef) of SLM-built samples subjected to isothermal holding at 170 °C, 244 °C and 290 °C, built on xy (a, b, c) and xz (d, e, f) planes.

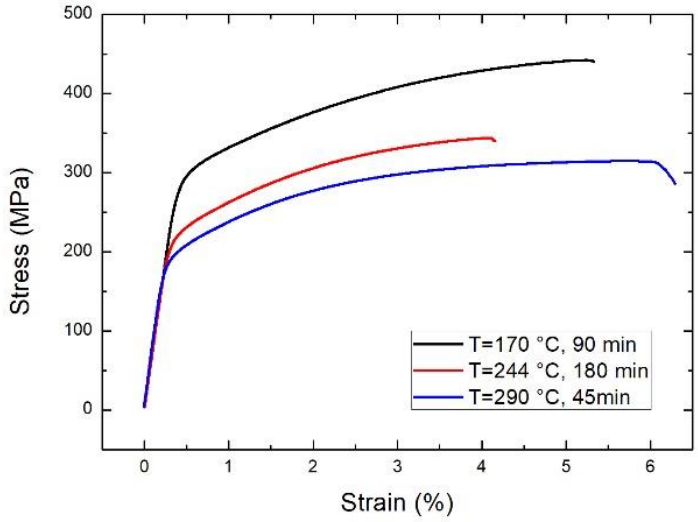

(a)

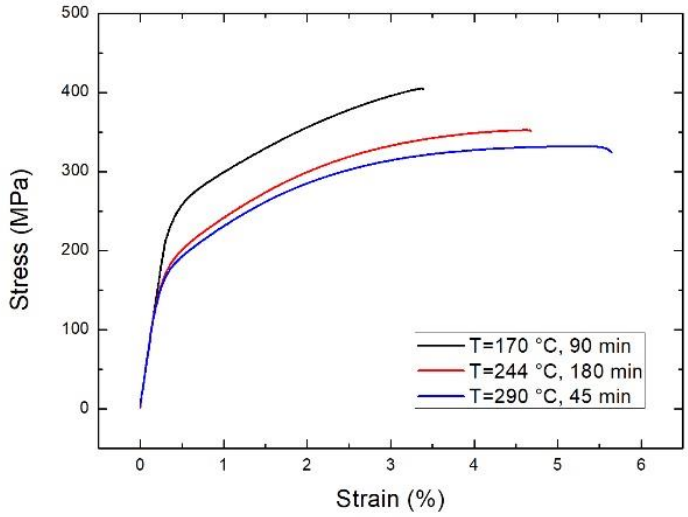

(b)

Figure 5: Tensile curves of AlSi10Mg samples built on a) xy (horizontal) and b) xz (vertical) planes, in the main heat treated conditions.

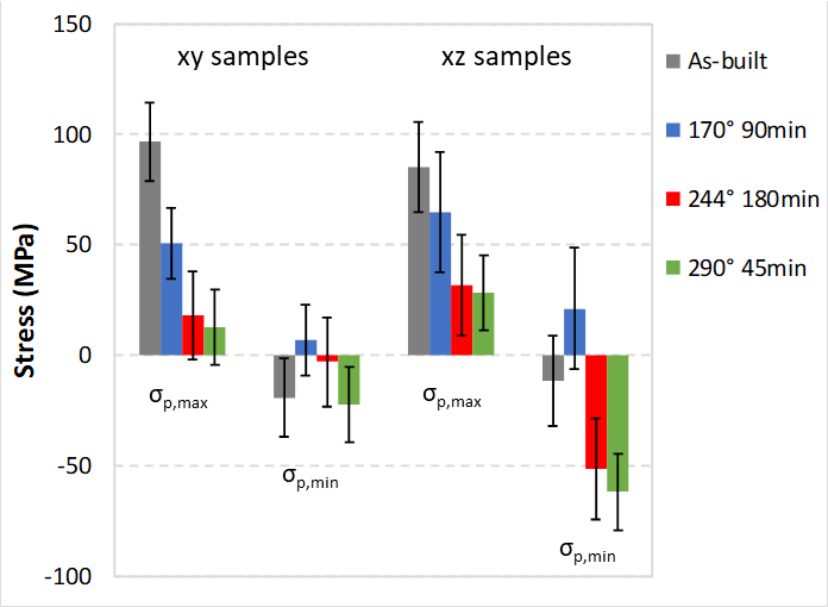

Figure 6: Maximum and minimum principal stresses in as-built and heat treated conditions, for xy and xz samples: mean and standard deviation.

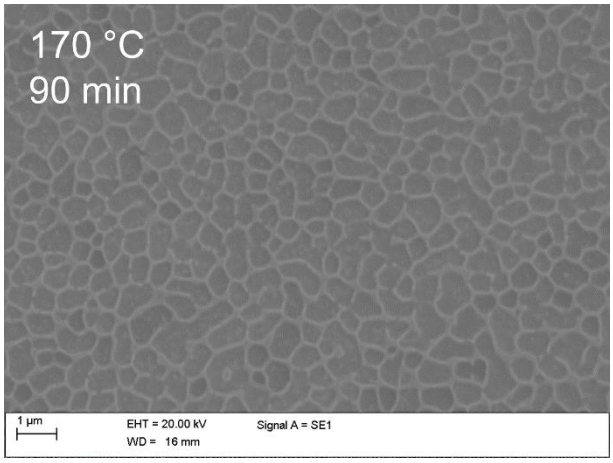

(a)

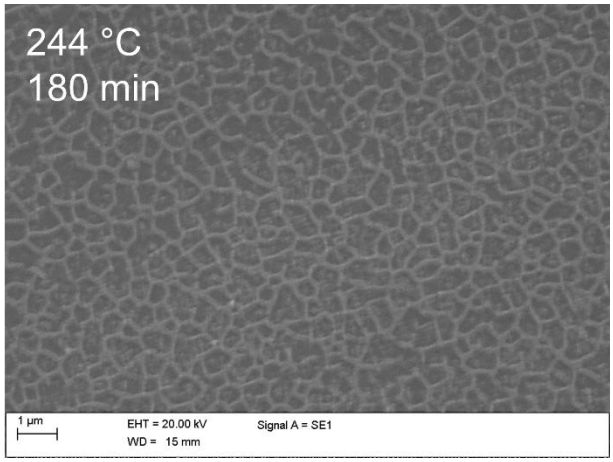

(b)

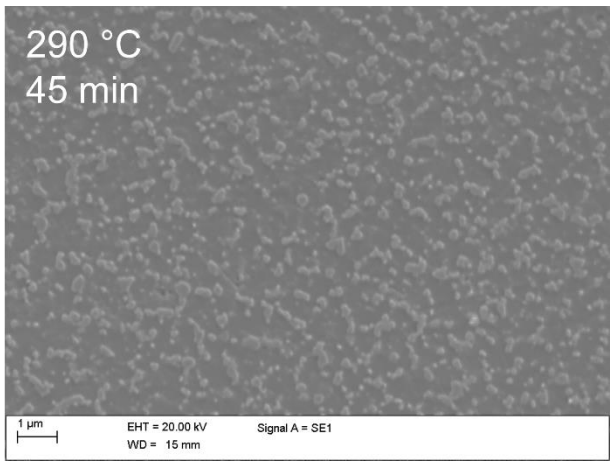

(c)

Figure 7: SEM micrographs of SLM built samples after heat treatment at 170 °C for 90 min, 244 °C for 180 min and 290 °C for 45 min. All images were taken on the xy plane in the fine fusion zone.

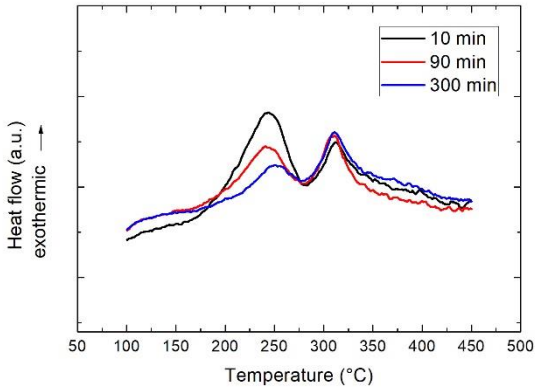
10 min
90 min
300 min
Heat flow (a.u.)
exothermic
50 100 150 200 250 300 350 400 450 500
Temperature (°C)

(a)

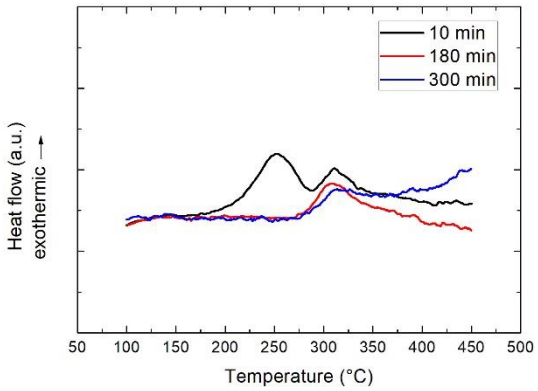
10 min
180 min
300 min
Heat flow (a.u.)
exothermic
50 100 150 200 250 300 350 400 450 500
Temperature (°C)

(b)

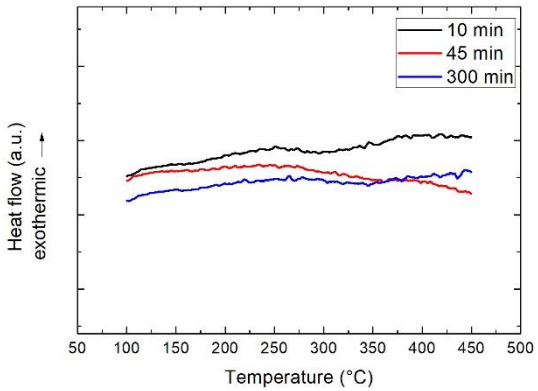
10 min
45 min
300 min
Heat flow (a.u.)
exothermic
50 100 150 200 250 300 350 400 450 500
Temperature (°C)

(c)

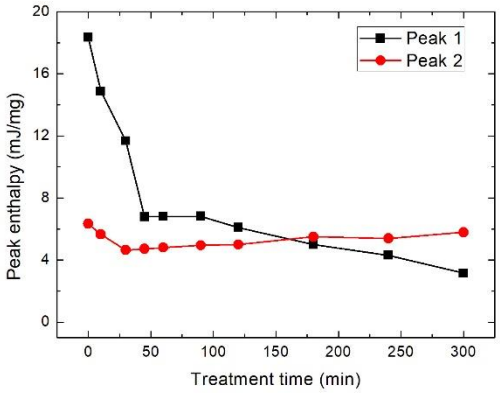

(d)

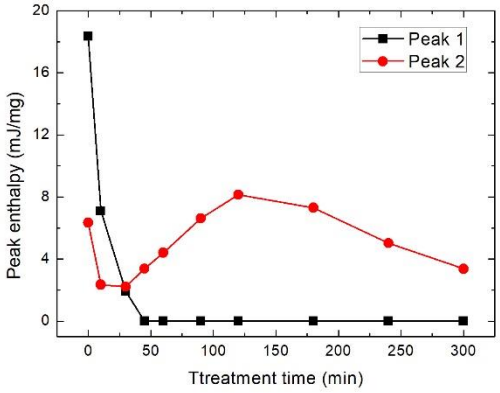

(e)

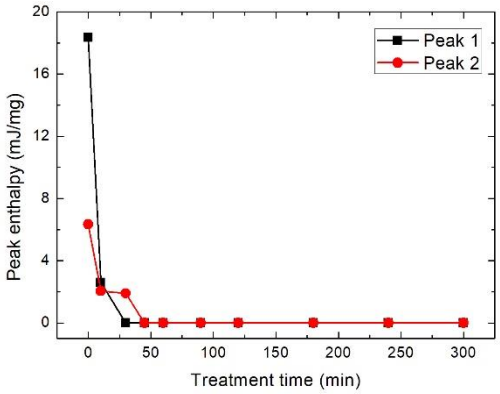

(f)

Figure 8: DSC curves recorded at 10 °C/min of samples heat treated for various times at a) 170 °C, b) 244 °C and c) 290 °C. Transformation enthalpies related to peak 1 and peak 2 in samples heat treated for various times at d) 170 °C, e) 244 °C and f) 290 °C.